Modeling and Monitoring of Polymorphic Transformations During the Drying Phase of Wet Granulation

Tiffani D. Davis,[1,2] Garnet E. Peck,[1] Joseph G. Stowell,[1] Kenneth R. Morris,[1,3] and Stephen R. Byrn[1]

Received December 26, 2003; accepted January 28, 2004

Purpose. The purpose of this work was to monitor polymorphic transformations of glycine during the drying phase of a wet granulation and model the polymorphic conversions using a time-based reconciliation model.

Methods. Near-infrared spectroscopy (NIR) was used for quantitation of polymorphs, and X-ray powder diffraction (XRPD) was used for qualitative analysis of polymorphs.

Results. The data show that the faster the granulation was dried, the more kinetic trapping of the metastable α-glycine polymorph, as predicted by reconciliation of the time scales of both the drying rate and the rate of the solution-mediated conversion.

Conclusions. By knowing basic properties of the drug substance (solubility of the polymorphic forms and the rate of the solution-mediated conversion), processing conditions, such as the drying rate, can be adjusted to anticipate and prevent potential polymorphic transformations.

KEY WORDS: fluid-bed drying; glycine; near-infrared spectroscopy; polymorphism; tray drying.

INTRODUCTION

Wet granulation is a size enlargement process during which small particles are formed into larger, physically strong agglomerates, using a binding agent (1). During a wet granulation, a solvent, usually with a polymeric binder, is added to wet the drug substance and excipients. Once the wetting phase is complete, the drug substance and excipients are dried. The combination of granulating solvent and drying conditions provide a suitable environment for the conversion to alternate crystalline forms. Crystal form conversions during the wet granulation process have been reported in the literature. Wong and Mitchell (2) found chlorpromazine hydrochloride converted from form II to form I via an intermediate hydrate phase during wet granulation in an ethanol:water (80.5:22.9 v/v) mixture. Form II transformed to a hemihydrate and then dehydrated to form I following drying at 70°C (2). Different forms of carbamazepine were found to convert to the dihydrate following a wet granulation. Upon drying at 60°C, the dihydrate converted into form III (3). Finally, the stable form A of fosinopril sodium was found to convert to the metastable form B following rapid drying of an alcoholic granulation (4).

Near-infrared (NIR) spectroscopy is a rapid, virtually nondestructive technique that requires minimal sample preparation. Absorption bands in the NIR arise from overtones or combinations from the vibrations in the mid-IR region and are 10–1000 times weaker than their fundamental bands in the mid-IR. Because polymorphs differ in the manner in which the molecules pack into the crystal lattice, they typically exhibit differences in hydrogen bonding. Differences in hydrogen bonding are observed as shifts in the fundamental bands in the mid-IR region and are readily observable as both overtones and combinations or the fundamental vibrations in the NIR. These differences in the NIR can then be exploited for the quantitation of polymorphs. Luner *et al.* (5) have shown accurate and precise quantitation of the crystalline forms of sulfamethoxazole, sulfathiazole, lactose, and ampicillin. Additionally, small amounts (0–10%) of sulfamethoxazole form I in form II (5) and sulfathiazole form I in form III (6) have been quantified using NIR. Patel, Luner, and Kemper (7) have also shown NIR useful in detecting low levels of polymorphs in multicomponent mixtures. They showed NIR could be used to quantify polymorphs in the range of 2–5%, even with significant levels of dilution with lactose.

Glycine was the model compound chosen for this study. Glycine may exist in three polymorphs: α, β, or γ glycine (8–11). β-Glycine is monotropically related to the α or γ form (12). The γ form is stable at room temperature, but slowly converts to the alpha form above 165°C (11,13). Near-infrared spectroscopy has been used to distinguish between the α and γ forms of glycine (14). The glycine polymorphs show differences in the C–H overtones and combination bands, as well as differences in the N–H stretch, NH_3^+ deformation and COO^- stretch, and will be discussed in detail in the "Results and Discussion" section.

The hypothesis being tested is that the time scales for both the processes of drying and solution-mediated conversion of polymorphs will determine the final polymorphic form.

MATERIALS AND METHODS

Materials

Glycine (Lot Nos. 7728 V16H16, 7728 V22478, 7728 T24473, 7728 N31476, 7728 V48472) was obtained from Mallinkrodt (Paris, KY, USA). Microcrystalline cellulose (PH 102, Lot No. 2521) was obtained from F.M.C. (Newark, DE, USA).

Methods

Preparation and Characterization of Polymorphs

γ-Glycine was obtained by re-crystallization of glycine as received from Mallinkrodt in either double-distilled water at twice the saturation solubility at 25°C or in 15% glacial acetic acid and water. The glycine solution was heated to approximately 70°C to dissolve all of the glycine, and then slowly cooled to room temperature without agitation. The resulting crystals were collected via vacuum filtration, and then ball-milled in a 4.5 L ceramic ball-mill with approximately 1 inch diameter ceramic balls for at least 24 h (Paul O. Abbé, Inc., Little Falls, NJ, USA). The ground crystals were then sieved

[1] Department of Industrial and Physical Pharmacy, Purdue University, West Lafayette, Indiana 48908-2091.

[2] Current address: Eli Lilly and Company, Indianapolis, Indiana 46285.

[3] To whom correspondence should be addressed. (e-mail: morriskr@purdue.edu)

0724-8741/04/0500-0860/0 © 2004 Plenum Publishing Corporation

using a Ro-Tap (Model RX-29, W.S. Tyler, Mentor, OH, USA), and only those crystals passing through the 90 μm sieve were used. All γ-glycine lots were blended together in a 16-quart twin shell V-blender, and the resulting blend was used for the calibration samples and granulations. α-Glycine was obtained by adding the as received glycine from Mallinkrodt to double-distilled water at approximately twice the saturation solubility at 25°C. The solution was then heated to 70°C in order to completely dissolve all of the glycine. This saturated solution was then cooled to room temperature with constant agitation, and the resulting crystals were collected by vacuum filtration. Only crystals passing through a 90-μm sieve were used.

Phase identification and purity of all polymorphs was assessed using X-ray powder diffraction and comparison with the calculated pattern. The calculated XRPD patterns were generated using Cerius[2] software from the corresponding single-crystal structures obtained from the Cambridge Structural Database (refcode: GLYCIN01 for gamma, and GLYCIN04 for alpha).

Preparation of Calibration Samples

Physical mixtures of glycine polymorphs were prepared by weight using a four-place analytical balance (Model AG 104, Mettler Toledo, Zurich, Switzerland). Calibration samples prepared for the granulation calibration model were diluted with 50% microcrystalline cellulose. For the glycine composition, mixtures ranged from 0% to 15% α-glycine in γ-glycine (0–7.5% overall with 50% dilution in microcrystalline cellulose). All compositions are further denoted by the percentage polymorph in the glycine portion. These samples consisted of 0%, 2.5%, 5%, 7%, 10%, 12.5%, and 15% α-glycine, with each percentage completed in triplicate. This percentage corresponds to the expected amount of polymorphic transformation during drying. Physical mixtures of glycine polymorphs undiluted with microcrystalline cellulose ranged from 0% to 100% α-glycine in γ-glycine in 10% intervals and was also completed in triplicate. A total sample weight of 500 mg was used, and all samples were prepared by geometric mixing of the sieved crystals. As α-glycine exists as bipyramids and γ-glycine exists as prisms (13), minimal segregation of the crystals should occur upon mixing. The samples were placed in one-dram screw-capped vials for NIR analysis.

Analytical Methods

Infrared spectra were acquired on a Magna-IR 860 Fourier transform infrared (FT-IR) spectrophotometer (Madison, Wisconsin) equipped with an Ever-Glo mid/far IR source, an extended range potassium bromide (KBr) beamsplitter, and a deuterated triglycine sulfate (DTGS) detector. A diffuse reflectance accessory (the Collector, Thermo Spectra-Tech) was used for sampling. Each spectrum represents 256 co-added scans collected at a spectral resolution of 4 cm^{-1}. Sample preparation consisted of mixing with KBr or analyzing as neat (as is), placing the sample into a 13-mm diameter cup, and leveling the material with a frosted glass slide. A background data set was acquired with an alignment mirror in place or on a sample of KBr. A Log 1/*R* (*R* = reflectance) spectrum was acquired by taking a ratio of these two data sets against each other. For KBr-diluted samples, the spectra were then converted to Kubelka-Munk units. Wavelength calibration was performed using polystyrene.

Near-infrared spectra were collected for quantitative measurement of polymorph content using a FOSS NIRSystems Model 6500-II Rapid Content Analyzer (FOSS NIRSystems, Silver Springs, MD, USA) over the wavelength range of 1100–2500 nm. Each spectrum was collected using 32 co-added scans, and the spectra were analyzed using Vision software (Version 2.51, FOSS NIRSystems, Inc.). Qualitative analysis of polymorph content was completed with X-ray powder diffraction using a Shimadzu XRD-6000 X-ray diffractometer (Kratos Analytical, Chestnut Ridge, NJ, USA). Diffraction patterns were collected using Cu Kα radiation over the range of 10°–40° 2θ, at a rate of 4° 2θ per minute with a step size of 0.04° (40 kV, 40 mA). On-line measurement of moisture content was determined using an MM55+ five wavelength filtering near-infrared spectroscopy gauge (NDC-Infrared Engineering, Irwindale, CA, USA) and calibrated using off-line measurements of moisture content. Offline measurement of moisture content was determined by loss on drying measurements between 85 °C and 100°C, using a Mettler Toledo LJ 16 moisture analyzer (Mettler Toledo Inc.). Differential scanning calorimetry (DSC) was performed on a TA instruments DSC analyzer (Model 2920, TA Instruments, New Castle, DE, USA). The sample was placed in an open aluminum pan under nitrogen purge (50 ml/min), with a heating rate of 10°C/min over the temperature range of 25–200°C. The DSC was calibrated with zinc and indium.

NIRS Analysis

Standard normal variate (SNV) mathematical treatment was applied to all spectra. The SNV transformation mean centers each NIR spectra to correct for baseline shifts due to particle size differences (15). The standard normal variation is calculated at each wavelength using Eq. 1.

$$SNV_{(1-700)} = (y_{(1-700)} - \bar{y}) / \sqrt{\frac{\sum (y_{(1-700)} - \bar{y})^2}{n-1}} \qquad (1)$$

where $SNV_{(1\text{-}700)}$ are the individual standard normal variations for 700 wavelengths, y is the 700-wavelength log 1/R values, and $\bar{y}$ is the mean of the 700-wavelength log 1/R values. The SNV transformed spectra were then further transformed into the second derivative of the response. The second derivative values were calculated using a second order finite-difference method with a segment size of 10 and gap size of 0. For this method, three segments at one end of the spectrum each separated by a gap are identified. The average absorbances are calculated for each segment (denoted as *A*, *B*, and *C*), and the second derivative value, computed as A – 2B + C, is assigned to the midpoint of the second segment. The segments and gaps are then shifted one data point, and the calculations are repeated until a second derivative value has been calculated for all of the data points in the spectrum.

A calibration model was constructed using a univariate inverse least squares method, represented by

$$C = B_o + B_1 R_i \qquad (2)$$

where C is the concentration, B_o is the intercept of the regression model, B_1 is the slope of the regression model, and R_i is the second derivative response at wavelength, λ_i. The cho-

sen analytical wavelength for the calibration model was based on interpretable differences in the NIR spectra, which also gave a high correlation coefficient, sensitivity and accuracy.

For the samples diluted with 50% MCC, a univariate inverse least squares calibration model was developed using the SNV plus second derivative transformation at 2152 nm. For the samples undiluted with MCC, a univariate inverse least squares calibration model was developed using the second derivative of the response plus SNV transformation at 2150 nm.

Solution-Mediated Conversion

The solution-mediated conversion of α-glycine to γ-glycine was measured under ambient conditions. For the solution-mediated conversion, α-glycine was added to a glycine-saturated solution, and the resulting slurry was continuously mixed. Slurries with 10% γ-glycine seeds were also completed. Samples were taken at various time intervals, filtered under vacuum using a büchner funnel, and then analyzed quantitatively with NIR and qualitatively with XRPD.

Solubility

The equilibrium solubility of both α-glycine and γ-glycine in water at 23°C was determined in triplicate by UV spectroscopy on a Cary 50 Bio UV-Vis Spectrophotometer (Varian, Australia) at 205 nm. The excess solid was analyzed with X-ray powder diffraction to ensure no transformation of α-glycine to γ-glycine had occurred during equilibration. No transformation was observed (not shown). The equilibrium solubility of γ-glycine was found to be 227.4 ± 2 mg/ml, whereas the equilibrium solubility of α-glycine was found to be 234.7 ± 2 mg/ml. Because a solution-mediated transformation did not complicate the analysis of the metastable form, this value is an accurate representation of the solubility.

Wet Granulations

Wet granulations were completed using 50% γ-glycine and 50% microcrystalline cellulose (MCC), with water as the granulating liquid. All granulations were wetted to 38% w/w moisture using a planetary mixer with paddle attachment (model N-50, Hobart Corp., Troy, OH, USA). After wetting, the wet mass was screened through a 12 mesh (1700 μm) screen, and then either placed in the Uni-Glatt fluid bed dryer (Glatt Air Products, Ramsey, NJ, USA) or spread out in an approximately ¼-inch to ½-inch layer on a 30 mesh (600 μm) screen, and tray dried at 21°C in a controlled, low humidity room (26–32% RH).

Fluid bed dried granulations were completed in triplicate at either 60°C or 80°C, using an inlet air flap angle between 20° and 25° for proper fluidization. Once drying was initiated, the fluid bed dryer was temporarily stopped every four minutes for sampling and offline analysis of polymorph content and moisture content. Throughout the drying process, online measurement of moisture content was also completed using the MM55 plus near-infrared spectrometer. A load size of 650 g was used for all granulations fluid bed dried at 60°C and one of the granulations fluid bed dried at 80°C. Two other granulations fluid bed dried at 80°C were completed using approximately 450 g of re-granulated material. A load size of 200 g was used for all tray-dried granulations. Continuous measurement of moisture content was also completed for the tray-dried granulations using the MM55 plus near-infrared spectrometer. Samples were also taken at various time intervals for offline analysis of both polymorph content and moisture content.

Prior to NIR analysis, all granulated samples were ground using an agate mortar and pestle, and approximately 500 mg of the ground material was then placed into a one-dram screw-capped vial. Because changes in particle size can shift the baseline of a NIR spectrum and decrease the predictive ability of the model, a study was completed to determine the best mathematical pretreatment for reducing particle size differences. In this study, a sample of the granulation was successively ground and re-analyzed. The mathematical pretreatment consistently giving the lowest variation was the SNV followed by the second derivative and was therefore used for the analysis of the granulated material. Loss on drying measurements for offline analysis of moisture content was completed using approximately 2–3 g of material.

RESULTS AND DISCUSSION

NIR Calibration Model

The glycine polymorphs have distinctly different NIR spectra (Fig. 1). The broad inflection points observed at approximately 1270 nm, 1600 nm, and 2050 nm are a result of bands from hydrogen-bonded N–H groups (14). The sharp peak observed for both forms of glycine around 1165 nm is due to the second overtone of the CH_2 stretch. NIR peaks observed in the 1660–1800 nm region, and between 2250 and 2450 nm are due to both combinations and overtones from CH_2 stretching. The distinct NIR band at approximately 2150 nm for α-glycine is a result of the differences in the crystal structures between α and γ-glycine (Fig. 2). Both crystal forms of glycine are composed of the zwitterionic glycine molecules. The intermolecular interaction responsible for stabilizing the crystal lattice are primarily N–H—O hydrogen bonds between ammonium nitrogens and carboxylate oxygens. In γ-glycine, all of the hydrogen bonds are linear, while in α-glycine, two hydrogens bond are linear and the third is bifurcated, or split between two hydrogen bond accepting carboxylate oxygens (14). The bifurcated hydrogen bond for α-glycine (H_{A3}) is weaker than the corresponding hydrogen bond for γ-glycine (H_{G3}), as evidenced by the longer hydro-

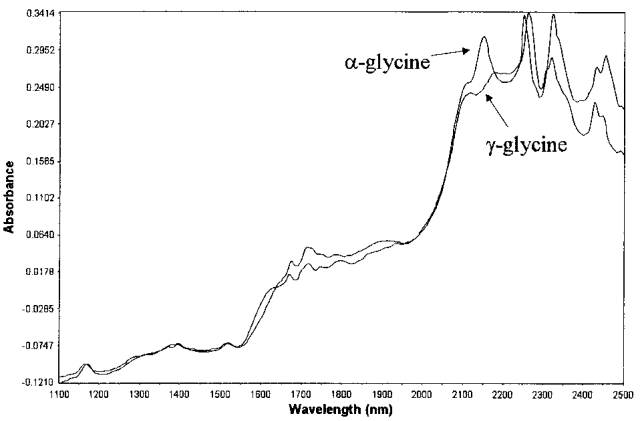

Fig. 1. Near-infrared reflectance spectra of α-glycine and γ-glycine.

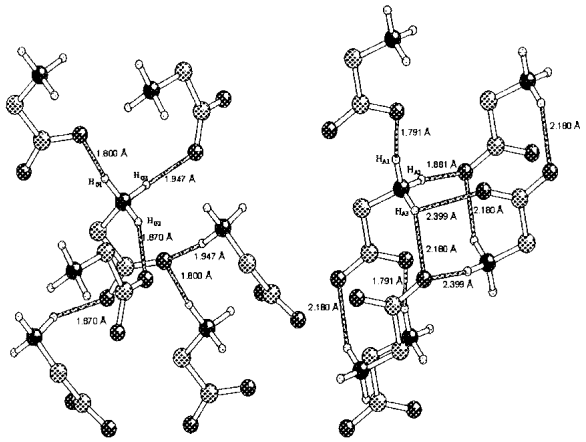

Fig. 2. Crystal structure for γ-glycine (left) and α-glycine (right).

gen bond lengths (2.399 Å and 2.180 Å for α-glycine and 1.947 Å for γ-glycine) and the differences in hydrogen bond angles (i.e., the more linear the hydrogen bond, in general, the stronger it is) (16). The weaker hydrogen bond attenuates the N–H stretching vibration less than the stronger bond. This has the effect of shifting the fundamental mid-IR frequency less so it appears at higher wavenumbers than in a strong hydrogen bond (i.e., more like the vapor state frequency).

As a result of the hydrogen bonding differences, the fundamental N–H stretch for α-glycine occurs at 3145 cm^{-1}, whereas the fundamental N–H stretch for γ-glycine occurs at 3120 cm^{-1}. The unique NIR peak for α-glycine at approximately 2147 nm (4658 cm^{-1}) is a combination band for the N–H stretch from the bifurcated hydrogen bond at 3145 cm^{-1} and NH_3^+ deformation at 1506 cm^{-1} (14). See Fig. 3 for the mid-IR spectra of both polymorphs.

When a diluent, such as microcrystalline cellulose is added to each form, it provides a background that also contributes to the spectral response. This is a result of the radiation being absorbed both by microcrystalline cellulose and glycine, with the remaining radiation being reflected and/or scattered. Nonetheless, the underlying features of each polymorph are retained and amplified by taking the second derivative of the NIR spectra (Fig. 4). As seen in Fig. 4, a distinct band for α-glycine centered at approximately 2152 nm is prominent in the second derivative spectra. The second derivative of NIR spectra is often used to resolve broad, overlapping peaks, and normalizes baseline shifts (17,18).

In a granulation, the drug substance and excipients undergo a particle size enlargement. However, all of the calibration samples used material less than 90 μm. In order to minimize the effects of particle size differences, all granulated samples were ground using an agate mortar and pestle. Because the particle size may still vary from sample to sample, the standard normal variate (SNV) (15), followed by calculating the second derivative was used to further minimize particle size differences. This mathematical pretreatment has previously been shown to give a high correlation coefficient and low standard error of calibration for a quantitative NIR assay (19).

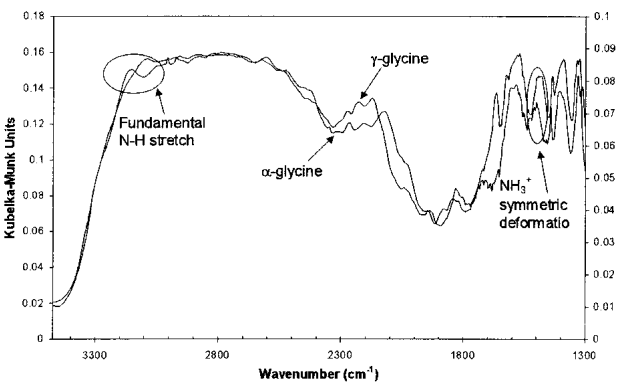

Fig. 3. Mid-IR spectra for α and γ-glycine.

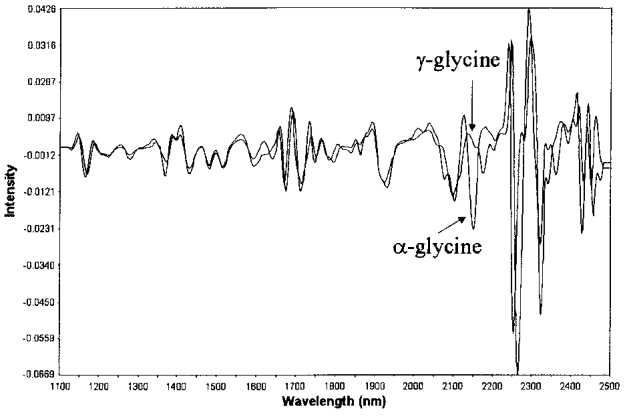

Fig. 4. The second derivative spectra for α and γ-glycine diluted with 50% microcrystalline cellulose.

A univariate inverse least squares calibration model using the SNV transformation followed by the calculation of the second derivative at 2152 nm was completed for the calibration samples. This model gave an R^2 value of 0.9920 and a standard error of calibration (SEC) of 0.4730. The SEC statistic is the standard deviation for the residuals between the actual and predicted values of the calibration samples. It can be calculated using Eq. 3.

$$SEC = \left[\frac{1}{N_T - n - 1} \sum_{i=1}^{N_T} (C_i - C_i')^2 \right]^{\frac{1}{2}} \quad (3)$$

where N_T is the number of samples in the calibration set, and n is the number of absorbance terms used in the regression model, C_i is the concentration of the analyte in the ith sample as calculated by the regression model, and C_i' is the true analyte concentration for the ith sample. Ideally, calibration models should have a large R^2 value and small SEC value (20).

A separate calibration model was also developed for α and γ-glycine without MCC. This model was developed to quantify the content of α-glycine during a solution-mediated conversion. A univariate inverse least squares calibration model was developed using the second derivative plus SNV transformation at 2150 nm. The chosen analytical wavelength for the calibration model was based on observable and interpretable differences in the NIR spectra, which also gave a high correlation coefficient, sensitivity, and accuracy. The model gave an R^2 of 0.9955 and a SEC of 2.19. Because this model covers a wide range of composition (0–100% α-glycine), a larger SEC would be expected for this model than for the model with MCC.

Wet Granulations

Assuming the temperature and pressure of the wetting process leave the polymorph within the stable region of the pressure-temperature phase diagram, the conversion of a stable to metastable form would not be expected to occur during the wetting phase of a wet granulation. However, after wetting, the amount of material in solution may be trapped as the metastable form. A conceptual model for transformations during drying is shown in Fig. 5. The stable form will go into solution at a rate proportional to its equilibrium solubility and its dissolution rate constant, k_{DSIII}. The solubility of the stable phase and the volume of the granulating solvent will determine the maximum amount of stable polymorph dissolved, and hence the maximum amount of metastable polymorph that may be trapped upon drying. After wetting, the material will be dried with a drying rate constant, k_{DRY}. If the drying rate is much faster than the solution mediated conversion of the metastable to stable form, the metastable polymorph may crystallize as drying progresses. In other words, if k_{DRY} is much faster than k_{DSI} and k_G, the metastable form will persist or be trapped upon drying. Additionally, the model assumes the excipients will provide a large number of sites for heterogeneous nucleation, thereby favoring rapid nucleation of the metastable form.

The maximum theoretical percent transformation of the metastable form can be calculated using

$$\textit{theoretical alpha } \% = \frac{V * 48 * C_s}{M} \tag{4}$$

where V is the volume of granulating liquid, C_s is the solubility of the stable form, and M is the mass of the stable form. From Eq. 4, the maximum theoretical percent α-glycine is calculated to be 13.6%. As seen in Eq. 4, it is assumed that 48% of the volume of granulating solution is available for the dissolution of γ-glycine. This quantity was experimentally determined by calculating the moisture content corresponding to the end of the heat transfer (evaporative) stage of drying, as this moisture amount should represent the "free" water on the surface of a granule. To determine the percentage of free water at the end of the heat transfer stage of drying, a loss on drying balance was used to obtain drying curves for three wetted samples of MCC. The point at which the drying process changes from linear to exponential (evaporative to diffusion limited) can be found by using a point-by-point linear regression on the appropriate equation until the correlation coefficient starts to decrease. From the point-by-point regression, the percentage free water was found to be 47.96 ± 1.8%.

The moisture and polymorph content of granulations dried in the fluid bed dryer are shown in Fig. 6. As the granulations dried, the α-glycine content rapidly increased and then remained fairly constant as drying progressed. This is also observed in the X-ray powder diffraction patterns run at each sampling interval throughout the drying process (not shown).

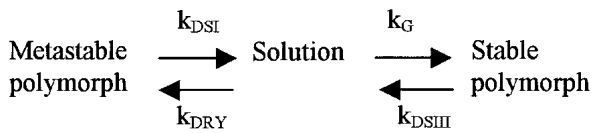

Fig. 5. Conceptual model for phase transformations during the drying phase of wet granulation.

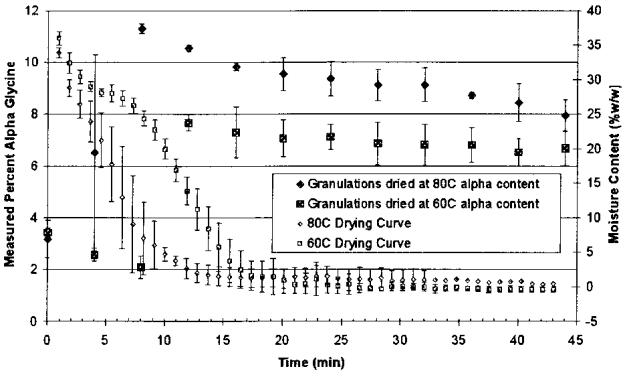

Fig. 6. Measured α-glycine percentage and moisture content for granulations fluid bed dried at 60°C and 80°C (error bars were determined from three repetitions).

Because NIR readily detects combination and overtones of OH stretching and bending vibrations of water molecules, the NIR spectrum of the wet granules (greater than 3% moisture content) displayed large, broad bands that interfered with the calculation of α-glycine polymorph content. This is evident by the large standard deviations seen in the wetted material. Therefore, analysis of polymorph content primarily focused on samples that contained less than 3% moisture content. From the fluid bed drying curve of the granulations at 80°C, the granules contain less than 3% moisture after approximately 12 min drying. Because fluid bed drying at 60°C is slower than at 80°C, the granulations dried at 60°C do not reach less than 3% moisture until approximately 16 min drying. The faster drying process also results in more α-glycine being trapped upon drying, with the content of the granules at 80°C exhibiting at least 2% more conversion than those dried at 60°C. The granules fluid bed dried at 80°C are distributed around 9.2% α-glycine content, while those dried at 60°C are scattered around 6.9% α-glycine.

The α-glycine content for the granules dried at 80°C, trends downward as the drying progresses. Because minimal water is present in the granules after the evaporative drying phase (less than 3%), a solution-mediated conversion would not be expected to occur. Additionally, this trend was not observed for the granules fluid bed dried at 60°C. DSC was run to determine if this phenomenon was due to a solid-solid conversion of α to γ-glycine. No endothermic or exothermic event was observed, indicating no solid-solid conversion. Therefore, the slight downward trend is likely due to error, such as sampling error.

Figure 7 shows the moisture and α-glycine content of the granules tray dried at room temperature. Just as with the fluid bed dried granules, to avoid error associated with large amounts of water content, the analysis of polymorph content focused on samples that contained less than 3% moisture content. Once dried, the α-glycine content is distributed around 0.9%. Thus, significantly less α-glycine is trapped after tray drying than after fluid bed drying.

Because fluid bed drying suspends and agitates material in a warm air stream, it is a more rapid drying process than tray drying. It is therefore expected that the granulating fluid would evaporate faster during fluid bed drying, resulting in a greater supersaturation of any dissolved material with respect to the metastable form, and a larger thermodynamic driving

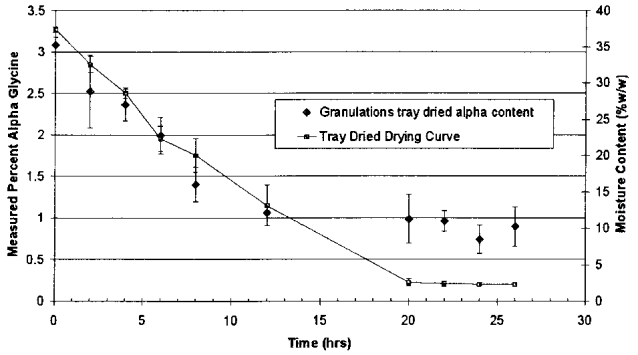

Fig. 7. Measured α-glycine content and moisture content for granulations tray dried at room temperature (error bars were determined from three repetitions).

force for the nucleation and crystallization of the metastable α-glycine. The relatively small difference in the solubilities of α and γ-glycine (234.7 ± 2 mg/ml and 227.4 ± 2 mg/ml, respectively), enable the solution to readily become supersaturated with respect to the α-form. During tray drying, an air stream also flows over the material. However, the material is not fluidized and consequently the drying process takes longer. The dissolved material is therefore expected to be less supersaturated with respect to either form, resulting in a smaller driving force for the crystallization of α-glycine. However, once crystallized, the α-glycine may convert to the more stable γ-glycine by a solution-mediated conversion, if given sufficient time in the granulating solvent. In other words, the balance between the drying rate and the rate of the solution-mediated conversion will determine the overall amount of α-glycine trapped after drying.

However, the solution mediated conversion rate is extremely slow for α-glycine, with slurries displaying no polymorph conversion during the time period of a drying cycle (less than 2 days), and one slurry showing no conversion after a month. Slurries with 10% γ-glycine seeds also occurred quite slowly. These slurries showed no conversion during the time frame of a drying cycle, and incomplete conversion until after 3 weeks. Because the solution-mediated conversion of α to γ-glycine is much longer than a drying cycle, any α-glycine trapped during drying will not convert to γ-glycine by a solution mediated process. Thus, the drying rate will determine the overall amount of metastable polymorph crystallized after drying.

CONCLUSIONS

The stable γ-glycine polymorph wet granulated with microcrystalline cellulose, and using water as the granulating solvent, displayed kinetic trapping of the metastable α-glycine after rapid drying in a fluid bed dryer. Slower drying techniques, such as tray drying, resulted in significantly less formation of α-glycine. The amount of polymorphic form was calculated using a NIR calibration model, which was shown to detect and quantify low levels of polymorph content. These results were further verified qualitatively using X-ray powder diffraction.

The total amount of α-glycine crystallized after drying is a combination of both the drying rate and the rate of the solution-mediated conversion of the metastable to stable form. Glycine was shown to have a very slow solution-mediated conversion, even in the presence of γ-glycine seeds. No conversion to the stable form occurred during the time frame of a typical drying cycle. Therefore, the drying rate determined the overall polymorph content. The faster the granulation was dried, the more rapid the increase in supersaturation with respect to the metastable form, and the greater thermodynamic driving force for the nucleation and crystallization of the metastable form. This was demonstrated by the significantly different polymorph contents from each drying condition. The granulations rapidly dried by fluidized bed drying resulted in more crystallization of α-glycine than the granulations that were tray dried. Additionally, the faster the fluidized bed granulations were dried, the more α-glycine crystallized.

The model assumes that only the metastable form nucleates and that the solution mediated conversion drives the appearance of γ-glycine. However, the rate of the solution-mediated conversion has shown to be insufficient, in conjunction with the model, to explain the observed appearance of γ-glycine at the various drying temperatures or supersaturation levels. The percentage of conversion can be predicted by plotting the percent conversion vs. the drying temperature. (The drying temperature will determine the overall level of supersaturation with respect to the metastable form.) This can be expressed in terms of the maximum theoretical conversion, based on the complete conversion of the material in solution, and the drying temperature by the following equation:

$$\textit{Actual Conversion} = \textit{Maximum Conversion} \times [1 - k(T)] \quad (5)$$

where $k(T)$ represents the difference between the maximum and actual conversion amounts as a fraction of the maximum. This generalized form potentially allows the prediction of the percent conversion by knowing the maximum theoretical conversion and $k(T)$.

Because polymorphs exhibit differences in chemical and physical stability, as well as mechanical and processing characteristics, polymorphic transformations during processes such as drying represent a significant impact for the pharmaceutical industry. However, by using advanced monitoring techniques, such as NIR, while also knowing basic properties of the drug substance (solubility of the polymorphic forms and the rate of the solution mediated conversion), processing conditions, such as the drying rate, can be adjusted to circumvent potential polymorphic disasters.

ACKNOWLEDGMENTS

The authors would like to acknowledge the NSF Industry University Cooperative Research Center for Pharmaceutical Processing for their financial support of this project.

REFERENCES

1. L. L. Augsburger and M. K. Vuppala. Theory of Granulation. In D. M. Parikh (ed.), *The Handbook of Pharmaceutical Granualation Technology*, Marcel Dekker, New York, 1997, pp. 7–8.
2. M. W. Y. Wong and A. G. Mitchell. Physicochemical characerization of a phase change produced during the wet granulation of chlorpromazine hydrochloride and its effects on tableting. *Int. J. Pharm.* **88**:261–273 (1992).
3. M. Otsuka, H. Hasegawa, and Y. Matsuda. Effect of polymorphic forms of bulk powders on pharmaceutical properties of carbamazepine granules. *Chem. Pharm. Bull.* **47**:852–856 ((1999)).

4. H. G. Brittain, K. R. Morris, D. E. Bugay, A. B. Thakur, and A. T. M. Serajuddin. Solid-state NMR and IR for the analysis of pharmaceutical solids: polymorphs of fosinopril sodium. *J. Pharm. Biomed. Anal.* **11**:1063–1069 (1993).
5. P. E. Luner, S. Majuru, J. J. Seyer, and M. S. Kemper. Quantifying crystalline form composition in binary powder mixtures using near-infrared reflectance spectroscopy. *Pharm. Dev. Tech.* **5**:231–246 (2000).
6. A. D. Patel, P. E. Luner, and M. S. Kemper. Low-level determination of polymorph composition in physical mixtures by near-infrared reflectance spectroscopy. *J. Pharm. Sci.* **90**:360–370 (2001).
7. A. D. Patel, P. E. Luner, and M. S. Kemper. Quantitative analysis of polymorphs in binary and multi-component powder mixtures by near-infrared reflectance spectroscopy. *Int. J. Pharm.* **206**:63–74 (2000).
8. G. Albrecht and R. B. Corey. Crystal structure of glycine. *J. Am. Chem. Soc.* **61**:1087–1103.
9. R. E. Marsh. A Refinement of the crystal structure of glycine. *Acta Cryst.* **11**:654–663.
10. Y. Iitaka. The crystal structure of γ-glycine. *Acta Cryst.* **14**:1–10.
11. Y. Iitaka. The crystal structure of β-glycine. *Acta Cryst.* **13**:35–45.
12. A. Peeters, C. Van Alsenoy, A. T. H. Lenstra, and H. J. Geise. Solids modeled by *ab initio* crystal field methods. X. Structure of α-glycine, β-glycine, and γ-glycine using a 15-molecular cluster. *J. Chem. Phys.* **103**:6608–6614 (1995).
13. I. Weissbuch, L. Leisorowitz, and M. Lahav. Tailor-made and charge-transfer auxilliaries for the control of the crystal polymorphism of glycine. *Adv. Mater.* **6**:952–956 (1994).
14. C. E. Miller and D. E. Honigs. Discrimination of different crystalline phases using near-infrared diffuse reflectance spectroscopy. *Spectroscopy* **4**:44–48 (1989).
15. R. J. Barnes, M. S. Dhanoa, and S. J. Lister. Standard normal variate transformation and de-trending of near-infrared diffuse reflectance spectra. *Appl. Spec.* **43**(5):772–777 (1989).
16. M. Falk and O. Knopp. In F. Franks (ed.), *Water: A Comprehensive Treatise*, Vol. 2, Plenum Press, New York, 1972, pp. 70–80.
17. L. G. Weyer. The use of derivative nodes in near-infrared spectroscopy, In C. S. Creaser and A. M. C. Davies (eds.), *Analytical Applications of Spectroscopy*, Royal Society of Chemistry, London, 1988, pp. 437–442.
18. J. D. Kirsch and J. K. Drennen. Near-infrared spectroscopy: applications in the analysis of tablets and solid pharmaceuticals dosage forms. *Appl. Spec. Rev.* **30**:139–174 (1995).
19. A. D. Trafford, R. D. Jee, A. C. Moffat, and P. Graham. A rapid quantitative assay of intact paracetamol tablets by reflectance near-infrared spectroscopy. *Analyst* **124**:163–167 (1999).
20. D. E. Honigs. Near infrared analysis. *Anal. Instr.* **14**(1):1–62 (1985).